

Fano effect on neutron elastic scattering by open-shell nuclei

K. Mizuyama¹, N. Nhu Le,^{2,3} and T. V. Nhan Hao^{2,4,*}

¹*Institute of Research and Development, Duy Tan University, Da Nang 550000, Vietnam*

²*Faculty of Physics, University of Education, Hue University, Hue City, Vietnam*

³*NTT Hi-Tech Institute, Nguyen Tat Thanh University, Ho Chi Minh City 700000, Vietnam*

⁴*Center for Theoretical and Computational Physics, University of Education, Hue University, Hue City, Vietnam*



(Received 12 September 2019; revised manuscript received 11 October 2019; accepted 18 February 2020; published 2 March 2020)

By focusing on the asymmetric shape of cross section, we analyze pairing effect on the partial wave components of cross section for neutron elastic scattering off stable and unstable nuclei within the Hartree-Fock-Bogoliubov framework. Explicit expressions for Fano parameters q_{lj} and ϵ_{lj} have been derived and pairing effects have been analyzed in terms of these parameters, and the Fano effect was found on the neutron elastic scattering off the stable nucleus in terms of the pairing correlation. The Fano effect appeared as the asymmetric line shape of the cross section caused by small absolute value of q_{lj} due to small pairing effect on the deep-lying hole state of stable nucleus. In the case of unstable nuclei, the large q_{lj} value is expected because of small absolute value of Fermi energy. The quasiparticle resonance with large q_{lj} forms Breit-Wigner-type shape in elastic-scattering cross section.

DOI: [10.1103/PhysRevC.101.034601](https://doi.org/10.1103/PhysRevC.101.034601)

I. INTRODUCTION

The Fano effect [1] has been known as a universal quantum phenomenon in which the transition probability becomes a characteristic asymmetric shape caused by the interference effect due to the correlation between discrete states (or resonance) and continuum. Many examples of Fano effect can be found in physics even though the mechanism is quite different for each example. Raman scattering [2,3], photoelectric emission [4], photoionization [5], photoabsorption [6], and neutron scattering [7] are examples which have been known in spectroscopy. Recently, in atomic and condensed matter physics, experimental research to control the Fano effect has been started [8,9] in order to investigate the detailed dynamical system of Fano effect. Also in nuclear physics, some observed resonances have been reported as candidate of the Fano resonance [10,11]; however, so far there has been no detailed study/analysis in terms of the Fano parameters.

In nuclear physics, sharp resonances found in the experimental data of $^{15}\text{N}(^7\text{Li}, ^7\text{Be})^{15}\text{C}$ reaction have been analyzed by using the channel-coupling equation and introduced as the candidates for the Fano resonance [10]. Another candidate for the Fano resonance in nuclei is quasiparticle resonance (or pair resonance) due to the particle-hole configuration mixing caused by pairing effect at the ground state of the open-shell nuclei. The experimental cross-section data of the $d(^9\text{Li}, ^{10}\text{Li})p$ reaction has been analyzed in terms of the effect of the pair resonance based on the Hartree-Fock-Bogoliubov (HFB) formalism [11]. Despite mentioning the possibility that these two candidates introduced in previous

studies are Fano effect, there was no detailed study on Fano parameters.

The aim of this study is to organize the Fano formula for neutron elastic scattering on the open-shell nuclei with the help of Jost function formalism [12] based on HFB [13], and we shall discuss the role of Fano parameters for the quasiparticle resonances seen in partial cross section of neutron elastic scattering. This is because characteristic asymmetric shapes of the cross sections have been shown as the numerical results obtained by the HFB framework [13].

First, we divide the Jost function into two parts: the scattering part and the pairing part. The Gell-Mann-Goldberger relation for the T matrix (expressed by the Jost function) has been obtained based on the HFB approach. Second, we derive explicit expressions of the Fano parameters q and ϵ for the neutron elastic scattering by open-shell nuclei within the HFB framework. Finally, the role of Fano parameters has been analyzed in comparison with the square of the T matrix plotted as a function of incident energy of neutron.

II. METHOD

A. Gell-Mann-Goldberger relation in HFB

The Jost function based on the HFB [13] can be divided as

$$[\mathcal{J}_{lj}^{(\pm)}(E)]_{s1} = \delta_{s1} J_{0,lj}^{(\pm)}[k_1(E)] \mp \frac{2m k_1(E)}{\hbar^2 i} \times \int dr \varphi_{0,lj}^{(\pm)}[r; k_1(E)] \Delta(r) \varphi_{2,lj}^{(rs)}(r; E), \quad (1)$$

using the Hartree-Fock (HF) solutions $\varphi_{0,lj}^{(\pm)}[r; k_1(E)]$ which satisfy the out-going/in-coming boundary conditions, and

*Corresponding author: tvnhao@hueuni.edu.vn

$\varphi_{2,lj}^{(rs)}(r; E)$ is the lower component of the HFB solution which is regular at the origin $r = 0$, where E is the quasiparticle energy and $k_1(E)$ is the momentum defined by $k_1(E) = \sqrt{\frac{2m}{\hbar^2}(\lambda + E)}$ with the Fermi energy $\lambda (< 0)$. $J_{0,lj}^{(\pm)}[k_1(E)]$ is the HF Jost function given by

$$J_{0,lj}^{(\pm)}[k_1(E)] = 1 \mp \frac{2m}{\hbar^2} \frac{k_1(E)}{i} \int dr r h_l^{(\pm)}[k_1(E)r] U_{lj}(r) \varphi_{0,lj}^r[r; k_1(E)], \quad (2)$$

where $U_{lj}(r)$ and $\Delta(r)$ are the HF mean field and the pair potential, respectively. We adopt the same Woods-Saxon form and their parameters as in Ref. [13] for numerical calculation. $\varphi_{0,lj}^r[r; k_1(E)]$ is the regular solution of the HF equation. $\varphi_{0,lj}^s[r; k_1(E)]$ and $\varphi_{0,lj}^{(\pm)}[r; k_1(E)]$ are connected by using $J_{0,lj}^{(\pm)}[k_1(E)]$ as

$$\varphi_{0,lj}^r[r; k_1(E)] = \frac{1}{2} \{ J_{0,lj}^{(+)}[k_1(E)] \varphi_{0,lj}^{(-)}[r; k_1(E)] + J_{0,lj}^{(-)}[k_1(E)] \varphi_{0,lj}^{(+)}[r; k_1(E)] \}. \quad (3)$$

From Eqs. (1) and (3), we derive

$$[\mathcal{J}_{lj}^{(-)}(E)]_{s1} J_{0,lj}^{(+)}[k_1(E)] - [\mathcal{J}_{lj}^{(+)}(E)]_{s1} J_{0,lj}^{(-)}[k_1(E)] = \frac{2m}{\hbar^2} \frac{2k_1(E)}{i} \int dr \varphi_{0,lj}^r[r; k_1(E)] \Delta(r) \varphi_{2,lj}^{(rs)}(r; E). \quad (4)$$

Applying the HFB T matrix given by Eq. (60) in Ref. [13] and the HF T matrix given by

$$\begin{aligned} T_{lj}^{(0)}(E) &= \frac{i}{2} \left\{ \frac{J_{0,lj}^{(-)}[k_1(E)]}{J_{0,lj}^{(+)}[k_1(E)]} - 1 \right\} \\ &= \frac{2mk_1(E)}{\hbar^2} \int_0^\infty dr r j_l[k_1(E)r] U_{lj}(r) \psi_{0,lj}^{(+)}[r; k_1(E)] \\ &= \frac{2mk_1(E)}{\hbar^2} \langle j_l[k_1(E)] | U_{lj} | \psi_{0,lj}^{(+)}[k_1(E)] \rangle \end{aligned} \quad (5)$$

to Eq. (4), we obtain

$$T_{lj}(E) - T_{lj}^{(0)}(E) = \frac{2mk_1(E)}{\hbar^2} \int dr \psi_{0,lj}^{(+)}[r; k_1(E)] \Delta(r) \psi_{2,lj}^{(+)}(r; E), \quad (6)$$

where $\psi_{0,lj}^{(\pm)}[r; k_1(E)] = \varphi_{0,lj}^r[r; k_1(E)] / J_{0,lj}^{(\pm)}[k_1(E)]$ and $\psi_{2,lj}^{(+)}(r; E)$ is the lower component of the HFB scattering wave function [13].

Equation (6) is the ‘‘Gell-Mann-Goldberger relation’’ (two potential formula) [14,15] in the HFB formalism. We can read that the right-hand side of Eq. (6) represents the transition from the holelike component (lower component) of the HFB scattering states to the HF scattering states caused by the pairing field $\Delta(r)$. The HFB scattering wave function $\psi_{lj}^{(+)}(r; E) = \begin{bmatrix} \psi_{1,lj}^{(+)}(r; E) \\ \psi_{2,lj}^{(+)}(r; E) \end{bmatrix}$ can be represented in the integral form

as

$$\begin{aligned} \begin{bmatrix} \psi_{1,lj}^{(+)}(r; E) \\ \psi_{2,lj}^{(+)}(r; E) \end{bmatrix} &= \begin{bmatrix} \psi_{0,lj}^{(+)}(r; k_1(E)) \\ 0 \end{bmatrix} \\ &+ \int dr' \begin{bmatrix} \mathcal{G}_{lj}^{11}(r, r'; E) & \mathcal{G}_{lj}^{12}(r, r'; E) \\ \mathcal{G}_{lj}^{21}(r, r'; E) & \mathcal{G}_{lj}^{22}(r, r'; E) \end{bmatrix} \\ &\times \begin{bmatrix} 0 & \Delta(r') \\ \Delta(r') & 0 \end{bmatrix} \begin{bmatrix} \psi_{0,lj}^{(+)}[r'; k_1(E)] \\ 0 \end{bmatrix}, \end{aligned} \quad (7)$$

using the HFB Green’s function given by 2×2 matrix form [16–18].

Inserting Eq. (7) into the right-hand side of Eq. (6), one obtains

$$\begin{aligned} T_{lj}(E) - T_{lj}^{(0)}(E) &= \frac{2mk_1(E)}{\hbar^2} \iint dr dr' \psi_{0,lj}^{(+)}[r; k_1(E)] \Delta(r) \\ &\times \mathcal{G}_{lj}^{22}(r, r'; E) \Delta(r') \psi_{0,lj}^{(+)}[r'; k_1(E)]. \end{aligned} \quad (8)$$

Since it has been proved that $S_{lj}^1(E)$ satisfies the unitarity on the scattering states defined on the real axis of E above the Fermi energy $-\lambda$ in Ref. [13], $S_{lj}^1(E)$ can be expressed as $S_{lj}^1(E) = e^{2i\delta_{lj}(E)}$. (The quasiparticle energy E is hereafter supposed to be on the scattering states.) Also $S_{lj}^{(0)}(E)$ can be expressed $S_{lj}^{(0)}(E) = e^{2i\delta_{lj}^{(0)}(E)}$ because of no absorption in $U_{lj}(r)$. Here, let us define a phase shift as $\delta_{lj}^{(1)} \equiv \delta_{lj} - \delta_{lj}^{(0)}$ to define $T_{lj}^{(1)} \equiv -e^{i\delta_{lj}^{(1)}(E)} \sin \delta_{lj}^{(1)}(E)$, and it may be rather trivial that $T_{lj}(E)$, $T_{lj}^{(0)}(E)$, and $T_{lj}^{(1)}(E)$ are related by

$$\begin{aligned} T_{lj}(E) &= T_{lj}^{(0)}(E) + T_{lj}^{(1)}(E) S_{lj}^{(0)}(E) \\ &= T_{lj}^{(0)}(E) [1 - iT_{lj}^{(1)}(E)] \\ &\quad + T_{lj}^{(1)}(E) [1 - iT_{lj}^{(0)}(E)]. \end{aligned} \quad (9)$$

B. Fano parameters

In this paper, we analyze the pairing effect on the partial cross sections of $p_{1/2}$ with $\lambda = -8.0$ MeV and $d_{3/2}$ with $\lambda = -1.0$ MeV by using the same Woods-Saxon parameters for the numerical calculation as in Ref. [13]. Both resonances are the so-called *hole-type* resonances originated from the hole state resulting from particle-hole (p-h) configuration mixing due to the pairing. As shown in Fig. 6 of Ref. [13], there is only one hole state for both $p_{1/2}$ and $d_{3/2}$ at the no-pairing limit.

In such cases, the Hartree-Fock-Green function can be expressed as

$$\begin{aligned} G_{\text{HF},lj}[r, r'; \epsilon(k)] &= \frac{\phi_{h,lj}(r) \phi_{h,lj}^*(r')}{\epsilon(k) - e_h} - i \frac{2mk}{\hbar^2} \psi_{0,lj}^{(+)}(r; k) \psi_{0,lj}^{(+)*}(r'; k) \\ &+ \frac{2m}{\hbar^2} \frac{2}{\pi} P \int_0^\infty dk' k'^2 \frac{\psi_{0,lj}^{(+)}(r; k') \psi_{0,lj}^{(+)*}(r'; k')}{k^2 - k'^2}, \end{aligned} \quad (11)$$

by dividing the continuum part into the principal and other parts in the spectral representation. Here $\epsilon(k) = \frac{\hbar^2 k^2}{2m}$.

Using Eq. (11), we obtain

$$\langle \phi_{h,lj} | \mathcal{G}_{lj}^{22}(E) | \phi_{h,lj} \rangle = \frac{1}{E - \lambda + e_h - F_{lj}(E) + i\Gamma_{lj}(E)/2}, \quad (12)$$

$$F_{lj}(E) = \frac{2m}{\hbar^2} \frac{2}{\pi} P \int_0^\infty dk' k'^2 \times \frac{|\langle \psi_{0,lj}^{(+)}(k') | \Delta | \phi_{h,lj} \rangle|^2}{k_1^2(E) - k'^2}, \quad (13)$$

$$\Gamma_{lj}(E)/2 = \frac{2mk_1(E)}{\hbar^2} |\langle \psi_{0,lj}^{(+)}[k_1(E)] | \Delta | \phi_{h,lj} \rangle|^2, \quad (14)$$

as an exact solution of the HFB Dyson equation for \mathcal{G}_{lj} .

Using Eqs. (8), (10), and (12), we derive

$$T_{lj}^{(1)}(E) = \frac{\Gamma_{lj}(E)/2}{E - \lambda + e_h - F_{lj}(E) + i\Gamma_{lj}(E)/2}. \quad (15)$$

When $\langle \psi_{0,lj}^{(+)}(k_1(E)) | \Delta | \phi_{h,lj} \rangle \neq 0$, we can obtain

$$\begin{aligned} 1 - iT_{lj}^{(0)}(E) &= \frac{\langle \psi_{0,lj}^{(+)}[k_1(E)] | \Delta | \phi_{h,lj} \rangle - iT_{lj}^{(0)}(E) \langle \psi_{0,lj}^{(+)}[k_1(E)] | \Delta | \phi_{h,lj} \rangle}{\langle \psi_{0,lj}^{(+)}[k_1(E)] | \Delta | \phi_{h,lj} \rangle} \\ &= \frac{\langle \psi_{0,lj}^{(+)}[k_1(E)] | \Delta | \phi_{h,lj} \rangle - \langle j_l[k_1(E)] | U_{lj} G_{\text{HF},lj}^* \Delta | \phi_{h,lj} \rangle}{\langle \psi_{0,lj}^{(+)}[k_1(E)] | \Delta | \phi_{h,lj} \rangle} \\ &\quad + \frac{2m}{\hbar^2} \frac{2}{\pi} P \int_0^\infty dk' k'^2 \frac{\langle j_l[k_1(E)] | U_{lj} | \psi_{0,lj}^{(+)}(k') \rangle \langle \psi_{0,lj}^{(+)}(k') | \Delta | \phi_{h,lj} \rangle}{[k_1^2(E) - k'^2] \langle \psi_{0,lj}^{(+)}[k_1(E)] | \Delta | \phi_{h,lj} \rangle}, \end{aligned} \quad (20)$$

by using Eqs. (5) and (11). Note that $\langle j_l[k_1(E)] | U_{lj} | \phi_{h,lj} \rangle = 0$ is also used.

Since $|\psi_{0,lj}^{(+)}(k)\rangle$ satisfies the Lippmann-Schwinger equation $|\psi_{0,lj}^{(+)}(k)\rangle = (1 + G_{\text{HF},lj} U_{lj}) |j_l(k)\rangle$, we rewrite Eq. (20) as

$$1 - iT_{lj}^{(0)}(E) = \frac{\langle j_l[k_1(E)] | \Delta | \phi_{h,lj} \rangle + \frac{2m}{\hbar^2} \frac{2}{\pi} P \int_0^\infty dk' k'^2 \frac{\langle j_l[k_1(E)] | U_{lj} | \psi_{0,lj}^{(+)}(k') \rangle \langle \psi_{0,lj}^{(+)}(k') | \Delta | \phi_{h,lj} \rangle}{k_1^2(E) - k'^2}}{\langle \psi_{0,lj}^{(+)}[k_1(E)] | \Delta | \phi_{h,lj} \rangle}. \quad (21)$$

Using Eq. (21), another parameter $q_{lj}(E)$ is defined by

$$q_{lj}(E) = \frac{1 - iT_{lj}^{(0)}(E)}{T_{lj}^{(0)}(E)}, \quad (22)$$

$$= \frac{\langle \chi_l[k_1(E)] | \mathcal{U}_{lj} | \Phi_{h,lj} \rangle}{T_{lj}^{(0)}(E) \langle \psi_{0,lj}^{(+)}[k_1(E)] | \Delta | \phi_{h,lj} \rangle}, \quad (23)$$

where

$$|\Phi_{h,lj}\rangle = \begin{bmatrix} |\Phi_{h,lj}^{(1)}\rangle \\ |\Phi_{h,lj}^{(2)}\rangle \end{bmatrix} = \begin{bmatrix} \frac{2m}{\hbar^2} \frac{2}{\pi} P \int_0^\infty dk' k'^2 \frac{|\psi_{0,lj}^{(+)}(k')\rangle \langle \psi_{0,lj}^{(+)}(k') | \Delta | \phi_{h,lj} \rangle}{k_1^2(E) - k'^2} \\ |\phi_{h,lj}\rangle \end{bmatrix}, \quad (24)$$

$$|\chi_l(k)\rangle = \begin{bmatrix} |j_l(k)\rangle \\ 0 \end{bmatrix}, \quad \mathcal{U}_{lj} = \begin{pmatrix} U_{lj} & \Delta \\ \Delta & -U_{lj} \end{pmatrix}. \quad (25)$$

This is the typical Breit-Wigner formula for the hole-type quasiparticle resonance. From this formula, we can notice that the hole state which satisfies $2\lambda - e_h - F_{lj}(E) > 0$ can be observed as the quasiparticle resonance in the neutron elastic scattering cross section since the incident neutron energy E_i is defined by $E_i = E + \lambda$.

One of the parameters introduced by U. Fano [1], $\epsilon_{lj}(E)$ is defined by

$$\epsilon_{lj}(E) = \frac{1 - iT_{lj}^{(1)}(E)}{T_{lj}^{(1)}(E)}, \quad (16)$$

$$= \frac{E - \lambda + e_h - F_{lj}(E)}{\Gamma_{lj}(E)/2}. \quad (17)$$

We notice that the quasiparticle resonance energy E_r and the width $\Gamma_{lj}(E_r)$ can be estimated as

$$\epsilon_{lj}(E = E_r) = 0, \quad (18)$$

$$\left. \frac{d\epsilon_{lj}(E)}{dE} \right|_{E=E_r} = \frac{2}{\Gamma_{lj}(E_r)}, \quad (19)$$

by using Eq. (17).

The upper component of $|\Phi_{h,lj}\rangle$ is originated from the admixture of a hole state and continuum due to the pairing. Note that Eq. (23) is quite analogous to Eq. (20) in Ref. [1].

C. Fano formula

Applying Eqs. (16) and (22) to Eq. (10), it is rather easy to obtain

$$T_{lj}(E) = -e^{i\delta_{lj}^{(1)}(E)} \frac{q_{lj}(E) + \epsilon_{lj}(E)}{\sqrt{1 + \epsilon_{lj}^2(E)}} T_{lj}^{(0)}(E). \quad (26)$$

Thus, we finally obtain the so-called *Fano formula*,

$$\frac{|T_{lj}(E)|^2}{|T_{lj}^{(0)}(E)|^2} = \frac{[q_{lj}(E) + \epsilon_{lj}(E)]^2}{1 + \epsilon_{lj}^2(E)}. \quad (27)$$

Using Eqs. (23) and (14), we obtain a very similar formula to Eq. (22) of Ref. [1],

$$q_{lj}^2(E)/2 = \frac{\hbar^2 k_1^2(E)}{2m} \frac{\frac{1}{\sqrt{k_1(E)}} \langle \chi_l | k_1(E) | \mathcal{U}_{lj} | \Phi_{h,lj} \rangle^2}{|T_{lj}^{(0)}(E)|^2 \Gamma_{lj}(E)}. \quad (28)$$

Since the resonance energy E_r is determined by Eq. (18) and $\Gamma_{lj}(E_r)$ is the width of the quasiparticle resonance, we obtain

$$\frac{|T_{lj}(E_r)|^2}{|T_{lj}^{(0)}(E_r)|^2} = q_{lj}^2(E_r), \quad (29)$$

$$= \frac{\frac{2m}{\hbar^2} \frac{1}{\sqrt{k_1(E_r)}} \langle \chi_l | k_1(E_r) | \mathcal{U}_{lj} | \Phi_{h,lj} \rangle^2}{|T_{lj}^{(0)}(E_r)|^2 \Gamma_{lj}(E_r)/2E_i^r}, \quad (30)$$

where $E_i^r = E_r + \lambda = \frac{\hbar^2 k_1^2(E_r)}{2m}$. The numerator of Eq. (30) is the transition probability to the “modified quasihole” state at the resonance E_r .

Therefore, $q_{lj}^2(E_r)/2$ is regarded as the ratio of the transition probabilities to the “modified quasihole” state $|\Phi_{h,lj}\rangle$ and to a scaled width $\Gamma_{lj}(E_r)/E_i^r$ of the HF continuum states $|\psi_{0,lj}^{(+)}\rangle$ at a quasiparticle resonance energy E_r .

As is well known, the characteristic features of the Fano formula Eq. (27) are

- (1) The shape of $|\frac{T_{lj}(E)}{T_{lj}^{(0)}(E)}|^2$ approaches the Breit-Wigner shape at the limit $|q_{lj}(E)| \rightarrow \infty$.
- (2) $|\frac{T_{lj}(E)}{T_{lj}^{(0)}(E)}|^2$ becomes zero at the energy $E = E_c$ which satisfies $q_{lj}(E_c) = -\epsilon_{lj}(E_c)$.

Also the parameter $q_{lj}(E)$ causes the asymmetric shape of $|\frac{T_{lj}(E)}{T_{lj}^{(0)}(E)}|^2$ in E as shown in Fig. 1 of Ref. [1] when the absolute value of $q_{lj}(E)$ is nonzero small value (see Fig. 1 of Ref. [1]), $q_{lj}(E)$ is, therefore, called “Fano asymmetry parameter” [19]. Besides, it is clear from Eq. (15) that $|T_{lj}^{(1)}(E)|^2$ always keeps the shape of the Breit-Wigner formula if a quasiparticle resonance exists.

III. NUMERICAL ANALYSIS

Numerical results for $p_{1/2}$ with $\lambda = -8.0$ MeV and $d_{3/2}$ with $\lambda = -1.0$ MeV are shown in Figs. 1 and 2, respectively, by adopting the Woods-Saxon potential for the mean-field potential and pair potential with same parameters as in Ref. [13].

In Figs. 1(a) and 2(a), the square of T matrix $|T_{lj}|^2$ and $|T_{lj}^{(0)}|^2$ of the neutron elastic scattering are plotted as a function of the incident neutron energy $E_i (= E + \lambda)$ by red curves and black curve. The solid red curve shows $|T_{lj}|^2$ with $\langle \Delta \rangle = 2.0$ MeV. The dashed and dotted curves are the same ones with $\langle \Delta \rangle = 2.5$ and 3.0 MeV, respectively. Corresponding phase shifts are shown in Figs. 1(b) and 2(b). In Figs. 1(c) and 2(c), $|T_{lj}|^2/|T_{lj}^{(0)}|^2$, which is representative of the quantity of the Fano formula Eq. (27). We show $|T_{lj}^{(1)}|$ represented by Eq. (15) in Figs. 1(d) and 2(d), and the corresponding phase shifts $\delta_{lj}^{(1)}$ are shown in Figs. 1(e) and 2(e). The Fano parameters q_{lj} and ϵ_{lj} are plotted by the solid black curve and the red curves in

Figs. 1(f) and 2(f). The dashed black curve represents $-q_{lj}$. The pairing dependence for all quantities in Figs. 1(b)–1(f) and Figs. 2(b)–2(f) is shown by solid, dashed, and dotted curves (corresponding to $\langle \Delta \rangle = 2.0, 2.5,$ and 3.0 MeV) as well as Figs. 1(a) and 2(a). The values of $E_r, \Gamma_{lj}(E_r), q_{lj}(E_r),$ and E_c for $p_{1/2}$ with $\lambda = -8.0$ MeV and $d_{3/2}$ with $\lambda = -1.0$ MeV are shown in Table I. It is confirmed that these values of E_r and $\Gamma_{lj}(E_r)$ match with the zeros of the absolute values of the Jost function on the complex energy plane shown in Ref. [13].

In Fig. 1, there is a dip at $E_i^c (= E_c + \lambda)$ and asymmetric shape in $|T_{lj}|^2$ [Fig. 1(a)] and $|T_{lj}|^2/|T_{lj}^{(0)}|^2$ [Fig. 1(c)]. Ac-

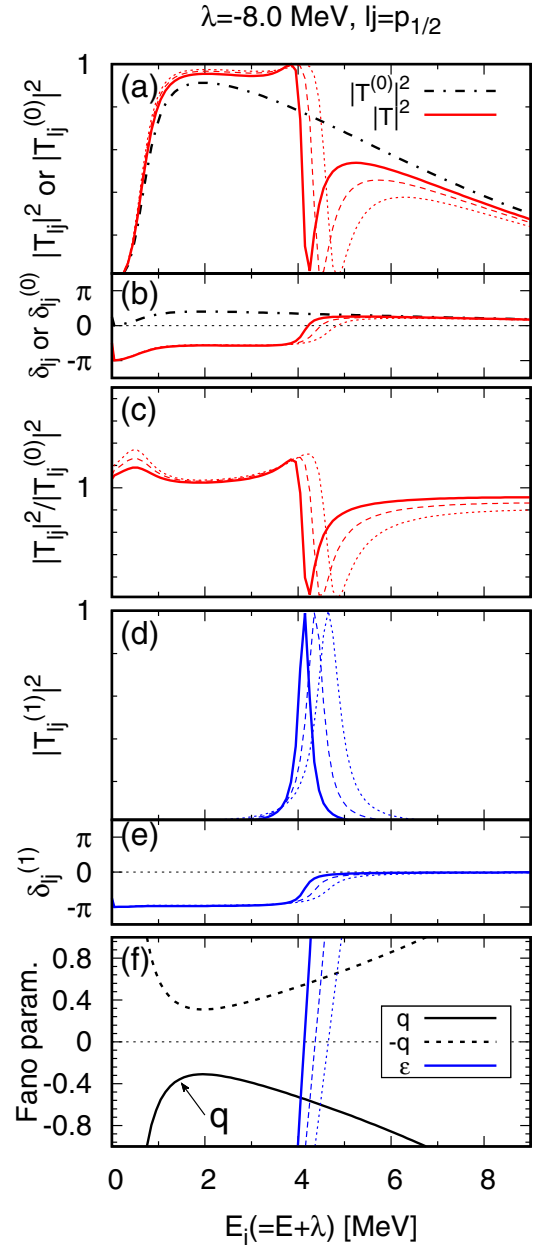


FIG. 1. The numerical results of square of T matrix of the neutron elastic scattering, corresponding phase shift, and the Fano parameters q and ϵ for $p_{1/2}$ plotted as a function of the incident neutron energy $E_i (= E + \lambda)$ with $\lambda = -8.0$ MeV. See text for details.

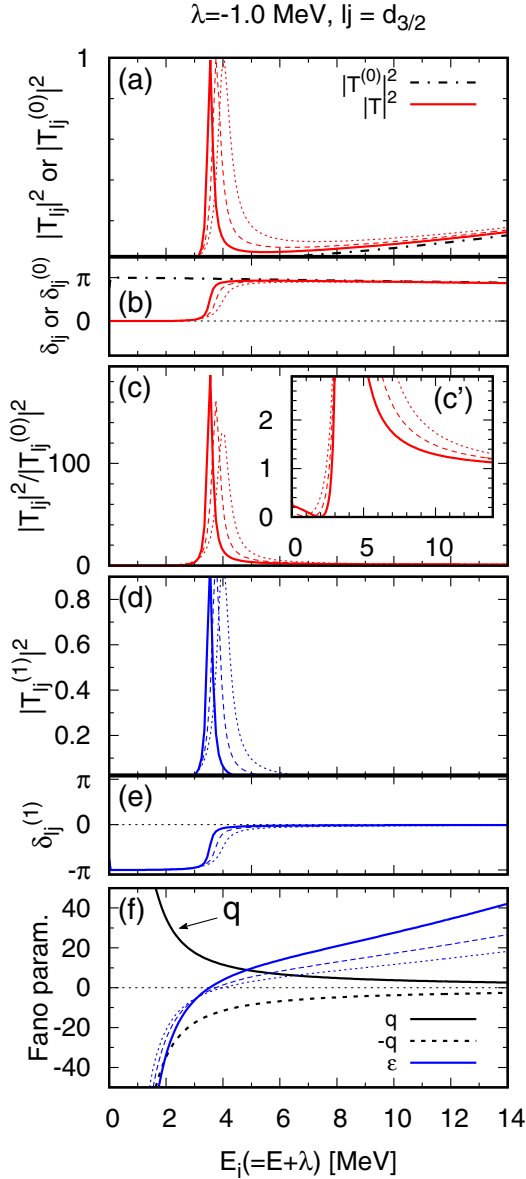


FIG. 2. Same with Fig. 1 but for $d_{3/2}$ with $\lambda = -1.0$ MeV.

According to the characteristic of the Fano formula Eq. (27), this asymmetric shape is due to the small absolute value of q_{lj} at the resonance energy E_r as shown in Fig. 1(f) and Table I. In Fig. 1(d), $|T_{lj}^{(1)}|^2$ shows a typical Breit-Wigner resonance shape representing a hole-type quasiparticle resonance originates from a deep-lying hole state ($e_{p_{1/2}} = -19.71$ MeV) due to the pairing correlation. The typical behavior of the phase shift for a resonance can be seen in Fig. 1(e). In Fig. 2, there is a sharp resonance in Figs. 2(a), 2(c) and 2(d). This resonance originates from a hole state at $e_{d_{3/2}} = -5.12$ MeV. According to the characteristic of the Fano formula Eq. (27), this is due to the large absolute value of q_{lj} at the resonance energy E_r as shown in Fig. 2(f) and Table I. The typical behavior of the phase shift for a resonance can be seen in Figs. 2(b) and 2(e).

In Table I, one can see that the energies E_r and E_c are shifted to higher energy, and the width $\Gamma_{lj}(E_r)$ becomes larger

TABLE I. The pairing gap dependence of E_r , $\Gamma_{lj}(E_r)$, $q_{lj}(E_r)$, and E_c for $p_{1/2}$ with $\lambda = -8.0$ MeV and $d_{3/2}$ with $\lambda = -1.0$ MeV. The energies E_r^i and E_c^i defined by $E_r^i = E_r + \lambda$ and $E_c^i = E_c + \lambda$ are shown in parenthesis. The results are shown in units of MeV except q_{lj} , q_{lj} is a dimensionless quantity.

| $\langle \Delta \rangle$ | $p_{1/2}$ ($\lambda = -8.0$ MeV) | | | $d_{3/2}$ ($\lambda = -1.0$ MeV) | | | |
|--------------------------|--------------------------------------|---------------|----------|--------------------------------------|----------------------|---------------|----------------------|
| | E_r (E_r^i) | Γ_{lj} | q_{lj} | E_c (E_c^i) | E_r (E_r^i) | Γ_{lj} | E_c (E_c^i) |
| 2.0 | 12.14 (4.14) | 0.28 | -0.55 | 12.21 (4.21) | 4.53 (3.53) | 0.20 | 13.80 (1.94) |
| 2.5 | 12.37 (4.37) | 0.42 | -0.58 | 12.49 (4.49) | 4.75 (3.75) | 0.34 | 12.67 (1.27) |
| 3.0 | 12.65 (4.65) | 0.56 | -0.63 | 12.84 (4.84) | 4.99 (3.99) | 0.52 | 11.55 (0.45) |

as the pairing gap $\langle \Delta \rangle$ increases. These are rather trivial pairing effects, because the energy shift F_{lj} and width Γ_{lj} are represented by Eqs. (13) and (14), and the pairing does not change the relative position between E_r and E_c . However, the pairing effect on $q_{lj}(E_r)$ is not so simple. In the case of $p_{1/2}$ with $\lambda = -8.0$ MeV, the absolute value of $q_{lj}(E_r)$ increases as the pairing gap $\langle \Delta \rangle$ increases. On the other hand, the absolute value of $q_{lj}(E_r)$ decreases as the pairing gap $\langle \Delta \rangle$ increases in the case of $d_{3/2}$ with $\lambda = -1.0$ MeV.

In order to clarify the pairing effect on $q_{lj}(E_r)$, we analyzed the pairing gap $\langle \Delta \rangle$ dependence of Eq. (30) in Fig. 3. The numerator of Eq. (30), the scaled width, and $|T_0(E_r)|^2$ are plotted as a function of the pairing gap $\langle \Delta \rangle$ in Figs. 3(a), 3(b) and 3(c), respectively. The red solid and blue dashed curves represent $p_{1/2}$ and $d_{3/2}$, respectively. The numerator of Eq. (30) and the scaled width increase as the pairing gap increases. The numerator of Eq. (30) for $d_{3/2}$ (with $\lambda = -1.0$ MeV) is larger than the one for $p_{1/2}$ (with $\lambda = -8.0$ MeV). This indicates that $d_{3/2}$ is more sensitive to the pairing than $p_{1/2}$ because $d_{3/2}$ is closer to the Fermi energy λ than $p_{1/2}$. In Fig. 3(b), the scaled widths show almost the same values and dependence on the pairing gap. The reason is rather trivial. As shown by Eq. (14), the width is expressed by the square of the coupling strength by pairing between the HF hole state and continuum. Therefore, the width should be similar value with the same pairing gap. Also, both quasiparticle resonances appear at the similar incident energies as shown in Table I. The $|T_0(E_r)|^2$ values for $p_{1/2}$ are much larger than the one for $d_{3/2}$. The difference of the $q_{lj}^2(E_r)$ between $p_{1/2}$ and $d_{3/2}$ is due to the difference of the ratios of the transition probability to the “modified quasihole” state and to the HF continuum between $p_{1/2}$ and $d_{3/2}$.

The small absolute value of $q_{lj}(E_r)$ for $p_{1/2}$ with $\lambda = -8.0$ MeV is due to the large value of the transition probability to the HF continuum and the small transition probability to the “modified quasihole” state because of the small pairing effect for the deep-lying hole state. However, the small absolute value of $q_{lj}(E_r)$ causes the asymmetric shape of the partial cross section of the neutron elastic scattering, which is known as a typical sign of the Fano effect.

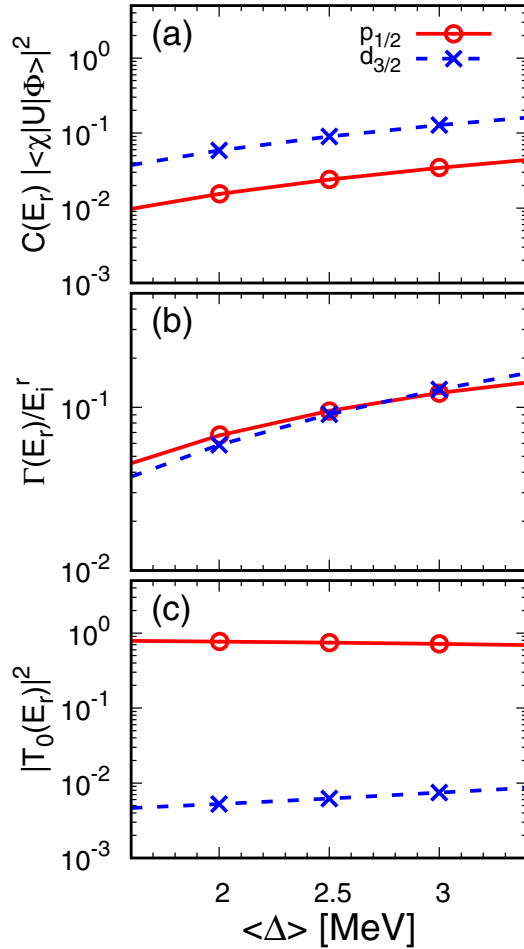


FIG. 3. The pairing gap $\langle \Delta \rangle$ dependence for the numerator of Eq. (30), the scaled width Γ/E_r^r , and $|T_0|^2$ are shown in panels (a), (b), and (c), respectively. The red solid and blue dashed curves represent $p_{1/2}$ with $\lambda = -8.0$ MeV and $d_{3/2}$ with $\lambda = -1.0$ MeV, respectively. A coefficient used for (a) is given by $C(E_r) = \left(\frac{2m}{\hbar^2}\right)^2 \frac{1}{k_1(E_r)}$.

On the other hand, the large absolute value of $q_{lj}(E_r)$ for $d_{3/2}$ with $\lambda = -1.0$ MeV is due to the small value of the transition probability to the HF continuum and the larger transition probability to the “*modified quasihole*” state. The hole $d_{3/2}$ state with $\lambda = -1.0$ MeV is much closer to the Fermi energy than $p_{1/2}$ with $\lambda = -8.0$ MeV at the zero pairing limit, and the $d_{3/2}$ state with $\lambda = -1.0$ MeV is more sensitive to the pairing effect. This is the reason of the larger transition probability to the “*modified quasihole*” state. The shape of the cross section for the quasiparticle resonance becomes the shape of the Breit-Wigner formula with the large $q_{lj}(E_r)$. More Breit-Wigner type resonances are therefore expected to be observed in the neutron elastic-scattering cross section on the neutron-rich open-shell nuclei.

IV. CONCLUSION

The Fano effect is known as a universal quantum interference effect between the sharp resonance (or discrete bound state) and continuum appears in the channel-coupling system including the particle-hole configuration mixing by pairing in the broad sense. In this paper, we have derived the Fano parameters within the HFB framework and analyzed the asymmetric shape of the quasiparticle resonance which appears on a partial wave component of the cross section for neutron elastic scattering off open-shell nuclei in terms of the Fano parameters. We found that, in case of the stable nucleus, the asymmetric shape of the cross section is due to the small absolute value of q_{lj} parameter because of the large transition probability to the HF continuum and small transition probability to the “*modified quasihole*” state. The latter transition probability is due to the weak pairing effect because the quasiparticle resonance for the stable nucleus originates from the deep-lying hole state. In contrast, the q_{lj} parameter for the quasiparticle resonance of unstable nucleus becomes large because of the small transition probability to the HF continuum and the large transition probability to the “*modified quasihole*” state due to the strong pairing effect. The shape of the cross section becomes the Breit-Wigner type with the large absolute value of q_{lj} parameter.

However, a coupling with other types of channel could also be the candidates of the origin of the Fano effect. It is already known that the channel coupling can be the origin of the sharp resonances on nucleon-nucleus elastic scattering [20–22]. Also, channel coupling originates the complex optical potential which gives a proper absorption for elastic scattering [21–24]. This proper absorption is important for the quantitative discussion of results in comparison with the experimental data. In addition, the correlation between different types of channel coupling are also expected. In order to investigate these points, we are planning the further extension of the Jost function by following two steps. As the first step, we will extend the Jost function formalism for the complex potential since the potential is supposed to be real in the current formalism. Second, we will extend the Jost function framework based on the particle-vibration formalism (including the pairing) in order to take into account the channel-coupling effect. Hopefully, we can discuss the existence of the Fano effect based on more realistic calculation and analysis in the near future.

ACKNOWLEDGMENTS

This work is funded by Vietnam National Foundation for Science and Technology Development (NAFOSTED) under Grant No. 103.04-2018.303.

[1] U. Fano, *Phys. Rev.* **124**, 1866 (1961).

[2] F. Cerdeira, T. A. Fjeldly, and M. Cardona, *Phys. Rev. B* **8**, 4734 (1973).

[3] V. Magidson and R. Beserman, *Phys. Rev. B* **66**, 195206 (2002).

[4] S. Hüfner, *Photoelectron Spectroscopy* (Springer-Verlag, Berlin, 1994).

- [5] U. Fano and A. R. P. Rau, *Atomic Collisions and Spectra* (Academic Press, San Diego, 1986).
- [6] J. Faist, F. Capasso, C. Sirtori, K. W. West, and L. N. Pfeiffer, *Nature* **390**, 589 (1997).
- [7] R. K. Adair, C. K. Bockelman, and R. E. Peterson, *Phys. Rev.* **76**, 308 (1949).
- [8] Christian Ott *et al.*, *Science* **340**, 716 (2013).
- [9] C.-M. Ryu and S. Y. Cho, *Phys. Rev. B* **58**, 3572 (1998).
- [10] S. E. A. Orrigo *et al.*, *Phys. Lett. B* **633**, 469 (2006).
- [11] S. Orrigo and H. Lenske, *Phys. Lett. B* **677**, 214 (2009).
- [12] R. Jost and A. Pais, *Phys. Rev.* **82**, 840 (1951).
- [13] K. Mizuyama, N. N. Le, T. D. Thuy, and T. V. Nhan Hao, *Phys. Rev. C* **99**, 054607 (2019).
- [14] M. Gell-Mann and M. L. Goldberger, *Phys. Rev.* **91**, 398 (1953).
- [15] L. F. Canto and M. S. Hussein, *Scattering theory of Molecules, Atoms and Nuclei* (World Scientific, Singapore, 2013).
- [16] M. Matsuo, *Nucl. Phys. A* **696**, 371 (2001).
- [17] S. A. Fayans, S. V. Tolokonnikov, E. L. Trykov, and D. Zawischa, *Nucl. Phys. A* **676**, 49 (2000).
- [18] S. T. Belyaev, A. V. Smirnov, S. V. Tolokonnikov, and S. A. Fayans, *Sov. J. Nucl. Phys.* **45**, 783 (1987).
- [19] K. Kato, Y. Hasegawa, K. Oguri, T. Tawara, T. Nishikawa, and H. Gotoh, *Phys. Rev. B* **97**, 104301 (2018).
- [20] A. M. Lane and R. G. Thomas, *Rev. Mod. Phys.* **30**, 257 (1958).
- [21] H. Feshbach, *Ann. Phys.* **5**, 357 (1958).
- [22] K. Mizuyama and K. Ogata, *Phys. Rev. C* **86**, 041603(R) (2012).
- [23] G. Blanchon, M. Dupuis, H. F. Arellano, and N. VinhMau, *Phys. Rev. C* **91**, 014612 (2015).
- [24] T. V. Nhan Hao, B. M. Loc, and N. H. Phuc, *Phys. Rev. C* **92**, 014605 (2015).